International Journal of Mechanical, Industrial and Aerospace Sciences
ISSN: 2517-9950
Vol:6, No:11, 2012

Flow and Heat Transfer Mechanism Analysis in Outward Convex Asymmetrical Corrugated Tubes

Huaizhi Han, Bingxi Li, Yurong He, Rushan Bie, and Zhao Wu

***Abstract*—**The flow and heat transfer mechanism in convex corrugated tubes have been investigated through numerical simulations in this paper. Two kinds of tube types named as symmetric corrugated tube (SCT) and asymmetric corrugated tube (ACT) are modeled and studied numerically based on the RST model. The predictive capability of RST model is examined in the corrugation wall in order to check the reliability of RST model under the corrugation wall condition. We propose a comparison between the RST modelling the corrugation wall with existing direct numerical simulation of Maaß C and Schumann U [14]. The numerical results pressure coefficient at different profiles between RST and DNS are well matched. The influences of large corrugation tough radii to heat transfer and flow characteristic had been considered. Flow and heat transfer comparison between SCT and ACT had been discussed. The numerical results show that ACT exhibits higher overall heat transfer performance than SCT.

***Keywords*—**Asymmetric corrugated tube, RST, DNS, flow and heat transfer mechanism.

I. Introduction

CORRUGATED tube named after the structures fabricated on the tube-wall can be categorized into two types based on the corrugated structures: inward concave corrugated tube and outward convex corrugated tube (studied in this paper). The proceeding method and relative merits of the two type tubes is presented in previous paper [1]. Corrugated tube is widely utilized in various heat exchangers to enhance heat transfer performance by intermittently destroying the momentum and thermal boundary layers on the inner and outer walls of it. Researches on the flow and heat transfer characteristics of corrugated tube have also been flourished in recent years. A large amount of studies (mostly experimental and also some numerical) have been carried out on the heat transfer enhancement performance of corrugated tubes (either helically corrugated tube or transverse corrugated tube), with consieration a variety of situations, such as Reynolds number effect [2-6], Prandtl number effects [3], wall roughness effect [4], entrance region [6], phase change flow [7,8], non-Newtonian fluid flow [9], ice slurry flow [10], overall performance of heat exchanger with use of corrugated tubes [11, 12], effects of ratios of pitch to pipe diameter, coil diameter to pipe diameter and length to pipe diameter [13], and so forth. For all the investigated situations, the consensus is that the analysis method heat transfer performance is mainly applied *Nu* (Nusselt number) and *f* (frictional factor). However, few investigations analysis the flow and heat transfer mechanism in corrugated tube. The heat transfer enhancement mechanism in the corrugated tube is described as follows. The periodically corrugated structure on the tube wall arouses periodic alteration of velocity gradient which leads to reverse pressure gradient locally. The recurrent alternation of axial pressure gradient of flow induces the secondary disturbance, and then the produced intensive eddy destroys the flow boundary layer and makes it thinner. The eddy also increases the turbulence intensity of the flow. The disturbance caused by corrugated structures thus increases the heat transfer coefficient drastically.

In this paper, a modified outward convex corrugated tube (SCT) was designed; the flow and heat transfer mechanism of it had been discussed.

Huaizhi Han, PhD Student, is with the School of Energy Science and Technology of Harbin Institute of Technology, Harbin 150090, Heilongjiang, China (phone: 86-451-86412155; e-mail: hanhz@hit.edu.cn).

Bingxi Li, Professor, Vice Dean, Corresponding author, is with the School of Energy Science and Technology of Harbin Institute of Technology, Harbin 150090, Heilongjiang, China (phone: 86-451-86412078; e-mail: libingx@hit.edu.cn).

Yurong He is with the School of Energy Science and Technology of Harbin Institute of Technology, Harbin 150090, Heilongjiang, China (e-mail: rong@hit.edu.cn).

Rushan Bie, Professor, is with the School of Energy Science and Technology of Harbin Institute of Technology, Harbin 150090, Heilongjiang, China

Zhao Wu, Master student, is with the School of Energy Science and Technology of Harbin Institute of Technology, Harbin 150090, Heilongjiang.

II. Numerical Simulation Procedures

A. Geometry of Outward Transverse Corrugated Tube and Meshing System

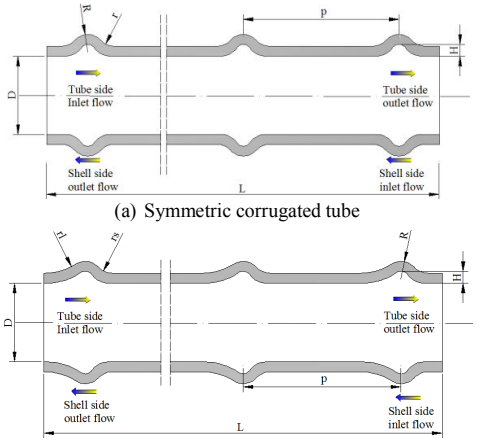

(a) Symmetric corrugated tube

(b) Asymmetric corrugated tube

Fig. 1 Structure parameters of outward transverse convex corrugated tube

Two kinds of outward convex transverse corrugated tube have been considered here, namely symmetric and asymmetric corrugated tubes (abbreviated as SCT and ACT, respectively), as shown in Fig. 1 together with the structure parameters. The structure parameters of the symmetric corrugated tub include inner diameter (D), tube length (L), corrugation height (H), corrugation pitch (p), corrugation crest radius (R) and corrugation trough radius (r). In order to save the computation cost, a section with L = 200 mm is cut from the whole tube as the computational domain. The only difference between the asymmetric and symmetric corrugated tubes is the corrugation trough radii. The corrugation trough radii of asymmetric corrugated tube on both sides are nominated respectively large corrugation trough radius (rl) and small corrugation trough radius (rs). Note that, since the investigated corrugated tubes are used in tube-shell type heat exchanger, the flow region out of tube is named "shell side".

TABLE I
MATERIAL PROPERTIES OF WORKING FLUIDS

Material	Density(ρ)/kg·m^{-3}	Specific heat(C_p)/J·kg^{-1}·K^{-1}	Thermal conductivity(λ)/W·m^{-1}·K^{-1}	Dynamic viscosity(μ)/kg·m^{-1}·s^{-1}
Helium	37.9293	5191	0.2724	3.46×10^{-5}

B. Governing Equations

The governing equations in a RANS (Reynolds Averaged Navier-Stokes) manner are given below.

Continuity equation:

$$\frac{\partial(\rho u_i)}{\partial x_i}=0 \tag{1}$$

Momentum equation:

$$\frac{\partial}{\partial x_j}\left(\rho u_i u_j\right)=-\frac{\partial p}{\partial x_i} + \frac{\partial}{\partial x_j}\left[\mu\left(\frac{\partial u_i}{\partial x_j}+\frac{\partial u_j}{\partial x_i}-\frac{2}{3}\delta_{ij}\frac{\partial u_j}{\partial x_j}\right)\right]+\frac{\partial}{\partial x_j}\left(-\rho\overline{u_i'u_j'}\right) \tag{2}$$

Energy equation:

$$\frac{\partial}{\partial x_i}\left[u_i\left(\rho E+P\right)\right]= \frac{\partial}{\partial x_i}\left[\left(\lambda+\frac{c_P\mu_t}{Pr_t}\frac{\partial T}{\partial x_i}\right)+\mu u_i\left(\frac{\partial u_i}{\partial x_j}+\frac{\partial u_j}{\partial x_i}-\frac{2}{3}\delta_{ij}\frac{\partial u_j}{\partial x_j}\right)\right] \tag{3}$$

The exact transport equations for the transport of the Reynolds stresses can be written as follows:

$$C_{ij}=D_{T,ij}+D_{L,ij}+P_{ij}+\phi_{ij}+\varepsilon_{ij} \tag{4}$$

$$C_{ij}=\frac{\partial}{\partial x_k}(\rho u_k\overline{u_i'u_j'}) \tag{5}$$

where the right hand side terms represent

$$D_{T,ij}=-\frac{\partial}{\partial x_k}\left[\rho\overline{u_i'u_j'u_k'}+\overline{p(\delta_{kj}u_i'+\delta_{ik}u_j')}\right] \tag{6}$$

$$D_{L,ij}=\frac{\partial}{\partial x_k}\left[\mu\frac{\partial}{\partial x_k}(\overline{u_i'u_j'})\right] \tag{7}$$

$$P_{ij}=-\rho(\overline{u_i'u_k'}\frac{\partial u_j}{\partial x_k}+\overline{u_j'u_k'}\frac{\partial u_i}{\partial x_k}) \tag{8}$$

$$\phi_{ij}=\overline{p(\frac{\partial u_i'}{\partial x_j}+\frac{\partial u_j'}{\partial x_i})} \tag{9}$$

$$\varepsilon=-2\mu\overline{\frac{\partial u_i'}{\partial x_k}\frac{\partial u_j'}{\partial x_k}} \tag{10}$$

$$D_{T,ij}=\frac{\partial}{\partial x_k}\left(\frac{\mu_t}{Pr_k}\frac{\partial\overline{u_i'u_j'}}{\partial x_k}\right) \tag{11}$$

Solve a transport equation for the turbulence kinetic energy in order to obtain boundary conditions for the Reynolds stresses. In this case, the following model equation is used:

$$\frac{\partial}{\partial x_i}(\rho k u_i)=\frac{\partial}{\partial x_i}\left[\left(\mu+\frac{\mu_t}{Pr_k}\right)\frac{\partial k}{\partial x_j}\right]+\frac{1}{2}P_{ii}-\rho\varepsilon \tag{12}$$

$$\frac{\partial}{\partial x_i}(\rho\varepsilon u_i)=\frac{\partial}{\partial x_j}\left[\left(\mu+\frac{\mu_t}{Pr_\varepsilon}\right)\frac{\partial\varepsilon}{\partial x_j}\right]C_{1\varepsilon}\frac{1}{2}\frac{\varepsilon}{k}P_{ii}-C_{2\varepsilon}\rho\frac{\varepsilon^2}{k} \tag{13}$$

The model constants $C_{1\varepsilon}$, $C_{2\varepsilon}$, C_μ, σ_k and σ_ε are chosen for the default values 1.44, 1.92, 0.09, 1.0 and 1.30, respectively.

C. Meshing system

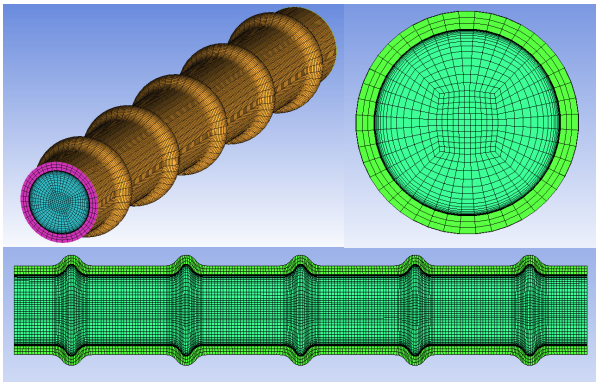

Fig. 2 Schematic diagram of mesh corrugated tube

A structured, non-uniform mesh system of hexahedra elements by ICEM is created in order to accurately control the size and number of cells in the domain as Fig. 2 shows. The vicinity of the near wall region presents the most important velocity and temperature gradients and because of that, grid clustering is required in the vertical direction near the walls to resolve the boundary layer. The dimension of the first cell next to the wall is determined by the Reynolds number and satisfies $y+\approx 1$ and the mesh spacing away from the wall increases with growth factor of 1.3 until the spacing becomes uniform in the main flow region where the value is 0.7mm in the radial direction. In order to predict and capture the detailed feature accurately and save the computational cost simultaneously, the values of the axial spacing in the corrugation region and the straight region are 0.5 mm and 0.7mm respectively.

D. Initial and Boundary Conditions

The flow boundary conditions on both sides are given as follows:

TABLE II
BOUNDARY CONDITIONS

Position	Type of boundary	Helium
Inlet	Velocity inlet	$V_{in,ts}$=20 m/s
		$Re_{in,ts}$= 25038
		$T_{in,ts}$=663.15K
		I_{ts}=5%
Outlet	Pressure	D_{ts}=20mm
		$P_{o,ts}$=3MPa
		I_{ts}=5%
		D_s=10mm
Tube	Wall	T_{ss}=600K
		coupled
		$T_{ts}=T_{w,ts}$
		$q_{ts}=q_{w,ts}$

E. Numerical Procedure

The governing equations are discretized by the finite volume method and solved by the steady-state implicit format. The SIMPLE algorithm is used to couple the velocity and pressure fields. The second-order upwind scheme is applied herein. The convergence criterion for energy is set to be 10-6 relative error and 10-4 relative error for other variables. The computations are carried out using ANSYS FLUENT 13.0, a commercial CFD package with a 2D configuration.

III. Result and Discussion

A. Validation of Simulation Model

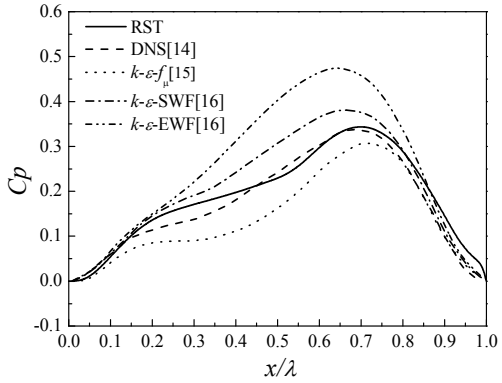

Fig. 3 Comparison of predicted Cp

The predicted results with RST model models are compared with the DNS data of Maaß and Schumann [14].The predicted pressure coefficients in the wave flat wall with RST model are compared to both DNS data are obtained by Cherukat et al. [15] and nonlinear k-ε-fμ model data are gained by Park et al. [16], in addition, k-ε-SWF and k-ε-EWF model by Hafez et al [17] as Fig. 3 shows. The value of Cp reflects the appearance of the favorable and adverse pressure gradient or the appearance of flow separation and reattachment in the case of a deep corrugated wall. As can be seen obviously in this figure, none of the models succeeded in predicting the pressure in the trough except the RMS-EWF model with little difference at the upstream of a wave. The nonlinear k-ε-fμ model underestimates the pressure coefficient all over the corrugation, whereas both k-ε-SWF and k-ε-EWF overestimates it, with the k-ε-SWF seems to be in better agreement with the DNS data than the k-ε-EWF. Finally, all calculation models show excellent pressure prediction near the wave crest.

B. Pressure Distribution Difference between ACT and SCT

Fig. 4 shows that pressure distribution for various large corrugation trough radii at tube side of ACT. The four graphs at tube side show that after a slightly favorable pressure gradient develops, the unfavorable pressure gradient occurs gradual earlier as increase of *rl* and gently upstream side gradient on the middle of corrugation. The maximum pressure drop which can be considered as reattachment point gradually augment as increase of the *rl* occurs on the downstream side of corrugation, and then favorable pressure gradient sustains on the whole downstream side. The separation phenomenon emerges once

again where the fluid passes downstream side of corrugation trough. The pressure drop maintains sustaining diminishing after entering the straight segment. The higher *rl* presents lower pressure drop at tube side.

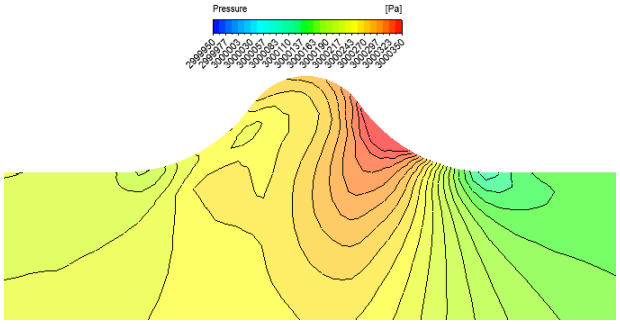

(a) *rl*=*rr*=5 (SCT)

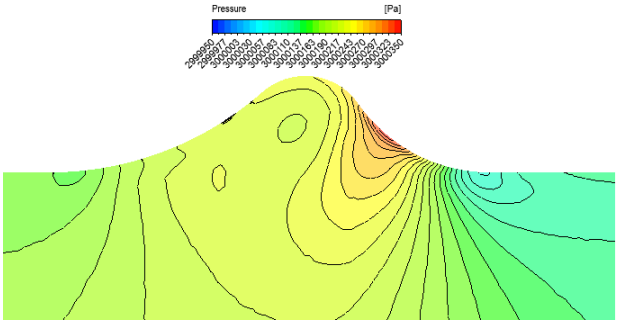

(b) *rl*=10, *rr*=5

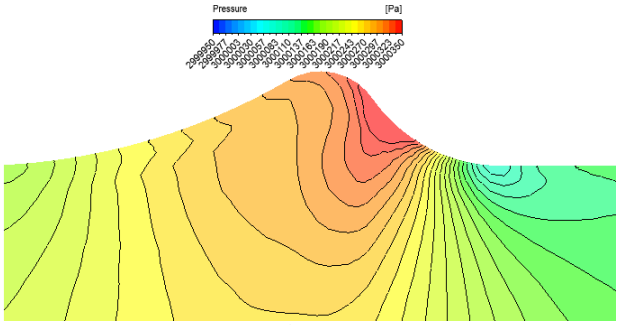

(c) *rl*=20, *rr*=5

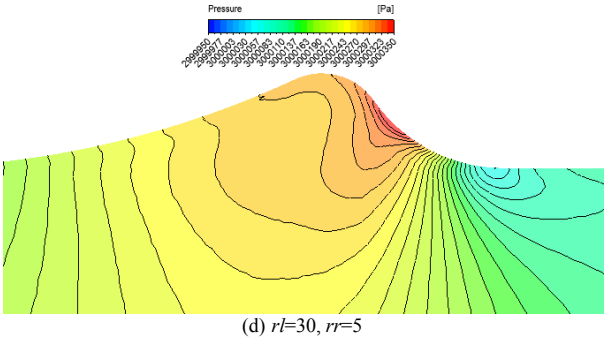

(d) *rl*=30, *rr*=5

Fig. 4 Pressure distribution for various large corrugation trough radii

C. Temperature Distribution Difference between ACT and SCT

From Fig. 5, it is seen that the thermal boundary layer grows thicker at the upstream of a corrugation. However, temperature gradient near the wall becomes larger at the downstream of corrugation tube. The thermal boundary layer starts to redevelops at the downstream of corrugation and grows thicker at the smooth segment; which lead to enhance the heat transfer in corrugated tube. Therefore, the heat transfer enhancement mainly focuses on the downstream of a corrugation. Compared with SCT, the thermal boundary layer thickness of ACT is thicker and which leading to the thermal efficiency slightly lower. The length of upstream of a corrugation is longer as increase of *rl,* and the length of thicken thermal boundary layer increases either, thus the heat transfer performance gradually decline as increase of *rl*.

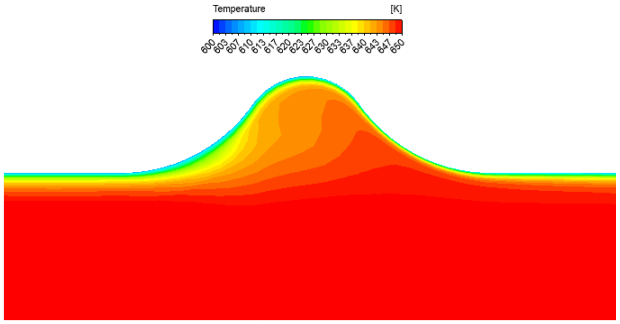

(a) *rl*=*rr*=5 (SCT)

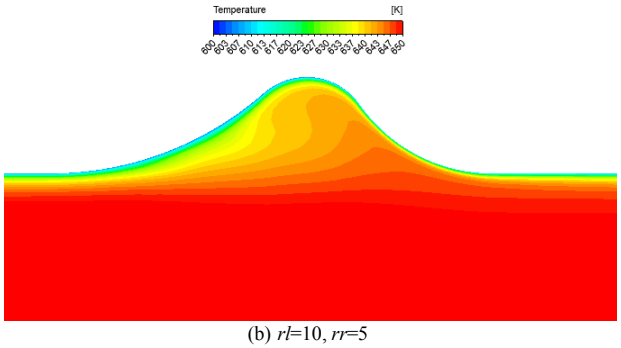

(b) *rl*=10, *rr*=5

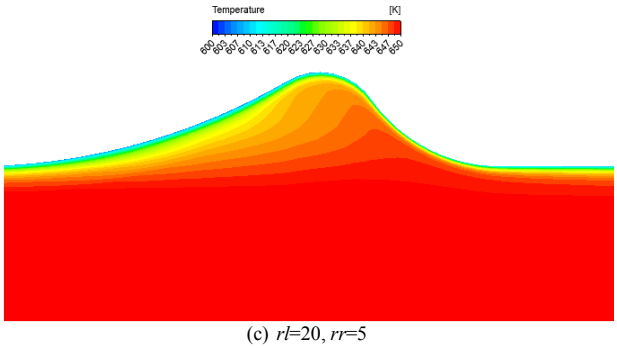

(c) *rl*=20, *rr*=5

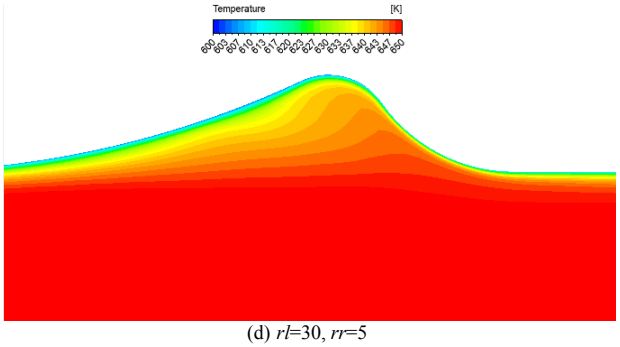

(d) *rl*=30, *rr*=5

Fig. 5 Pressure distribution for various large corrugation trough radii

D.Temperature Distribution Difference between ACT and SCT

Fig. 6 shows that Reynolds shear stress $\overline{u'v'}$ distribution for various large corrugation trough radii at tube side of ACT. In the case *rl*=*rs*=5mm, the magnitude of highest $\overline{u'v'}$ mainly focus on the region where fluid just leave the separation point and enter the reattachment point. The magnitude of $\overline{u'v'}$ in vortex center is less than the region previously mentioned. As increase of *rl*, the magnitude of $\overline{u'v'}$ gradually migrates toward the downstream side of corrugation and that at the upstream side of corrugation appears gradually attenuation. The $\overline{u'v'}$ decline results in decrease of pressure drop in the tube side. The overall heat transfer performance increase due to obvious decrease of pressure drop, although heat transfer performance decrease slightly.

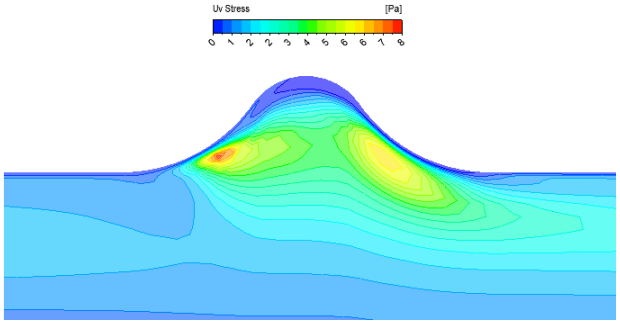

(a) *rl*=*rr*=5 (SCT)

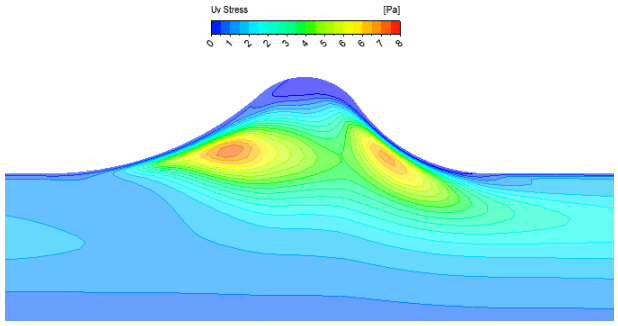

(b) *rl*=10, *rr*=5

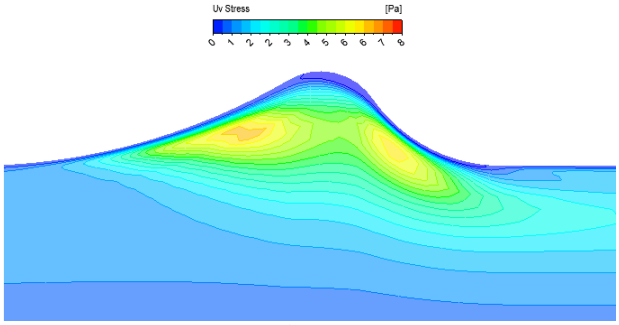

(c) *rl*=20, *rr*=5

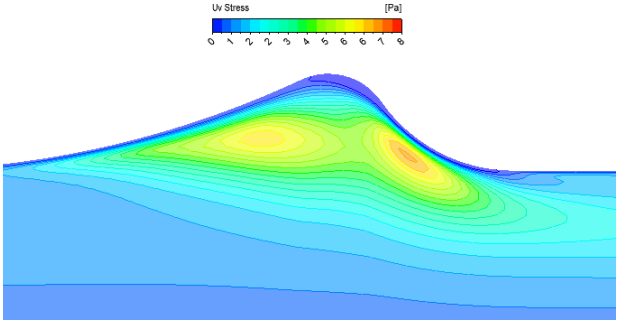

(d) *rl*=30, *rr*=5

Fig. 6 $\overline{u'v'}$ distribution for various large corrugation trough radii

IV. Conclusion

1. For the wavy flat wall, the RST model validation is made by comparing with the DNS data of Maaß C and Schumann U. The predicted results were in generally good agreement with the DNS data. Therefore, the RST model is applied to simulate in the corrugated tube.

2. The unfavorable pressure gradient occurs gradual earlier as increase of rl and gently upstream side gradient on the middle of corrugation. The maximum pressure drop which can be considered as reattachment point gradually augment as increase of the rl occurs on the downstream side of corrugation

3. The length of upstream of a corrugation is longer as increase of rl, and the length of thicken thermal boundary layer increases either, thus the heat transfer performance gradually decline as increase of rl.

4. The decline results in decrease of pressure drop in the tube side. The overall heat transfer performance increase due to obvious decrease of pressure drop, although heat transfer performance decrease slightly.

Nomenclature

C_p	Constant pressure specific heat capacity (J kg^{-1} K^{-1})
D	Inner diameter of tube (m)
f	Friction coefficient
H	Wave height (m)

L	Tube length (m)
Nu	Nusselt number (－)
P	Pressure (Pa)
Pr	Prandtl number(－)
p	Corrugation pitch (m)
R	Corrugation crest radius (m)
Re	Reynolds number(－)
r	Corrugation trough radius (m)
rl	Large corrugation trough radius (m)
rs	Small corrugation trough radius (m)
T	Temperature (K)
u	Velocity (m s^{-1})

Greek letters

α	Convective heat transfer coefficient (W m^{-2})
λ	Thermal conductivity (W $m^{-1}K^{-1}$)
μ	Dynamic viscosity (kg m^{-1} s^{-1})
ρ	Density (kg m^{-3})
τ	Total Stress (Pa)
k	Turbulence kinetic energy (m^2s^{-2})
□	Turbulence dissipation rate (m^3/s^{-2})

Superscripts

′	Fluctuating component

Subscripts

c	Corrugated tube
in	Inlet
i, j, k	Direction of coordinate
lam	Laminar
o	Outlet
t	Turbulence
ts	Tube side
s	Smooth tube
ss	Shell side
w	Tube wall

Abbreviations

ACT	Asymmetric corrugated tube
CFD	Computational fluid dynamics
SCT	Symmetric corrugated tube
RANS	Reynolds-averaged Navier-Stokes
RST	Reynolds stress transport

ACKNOWLEDGMENT

The authors gratefully acknowledge the support by Special fund of international technological cooperation and communication. (No. 2009DFR60120).

REFERENCES

[1] H.Z. Han, B.X. Li, B.Y. Yu, Y.R. He, F.C. Li. Numerical study of flow and heat transfer characteristics in outward convex corrugated tubes, International Journal of Heat Mass Transfer. Publication on line, 2012.
[2] S. Pethkool, S. Eiamsa-ard, Turbulent heat transfer enhancement in a heat exchanger using helically corrugated tube, International Communications in Heat and Mass Transfer 38 (2011) 340-347.
[3] P.G. Vicente, A. Garcia, A. Viedma, Experimental investigation on heat transfer and frictional characteristics of spirally corrugated tubes in turbulent flow at different Prandtl numbers, International Journal of Heat and Mass Transfer 47 (2004) 671-681.
[4] S. Rainieri, G. Pagliarini, Convective heat transfer to temperature dependent property fluids in the entry region of corrugated tubes, International Journal of Heat and Mass Transfer 45 (2002) 4525-4536.
[5] S. Rozzi, R. Massini, G. Paciello, Heat treatment of fluid foods in a shell and tube heat exchanger: comparison between smooth and helically corrugated wall tubes, Journal of Food Engineering 79 (2007) 249-254.
[6] G. Fabbri, R. Rossi, Analysis of the Heat Transfer in the Entrance Region of Optimized Corrugated Wall Channel, International Communications in Heat and Mass Transfer, 32 (2005) 902-912.
[7] L. Suriyan, W. Somchai, The effects of corrugation pitch on the condensation heat transfer coefficient and pressure drop of R-134a inside horizontal corrugated tube, International Journal of Heat and Mass Transfer 53 (2010) 2924-2931.
[8] K. Aroonrat, S. Wongwises, Evaporation heat transfer and friction characteristics of R-134a flowing downward in a vertical corrugated tube, Experimental Thermal and Fluid Science 35 (2011) 20-28.
[9] A. Barba, S. Rainieri, M. Spiga, Heat transfer enhancement in a corrugated tube, International Communications in Heat and Mass Transfer 3 (2002) 313-322.
[10] F. Illa´n, A. Viedma, Prediction of ice slurry performance in a corrugated tube heat exchanger, International Journal of Refrigeration, 32 (2009) 1302-1309.
[11] A. Zachár, Analysis of coiled-tube heat exchangers to improve heat transfer rate with spirally corrugated wall, International Journal of Heat and Mass Transfer 53 (2010) 3928-3939.
[12] N. Ghorbani, H. Taherian, M. Gorji, H. Mirgolbabaei, Experimental study of mixed convection heat transfer in vertical helically coiled tube heat exchangers, Experimental Thermal and Fluid Science, 34 (2010) 900-905.

[13] M. Moawed, Experimental investigation of natural convection from vertical and horizontal helicoidal pipes in HVAC applications, Energy Conservation and Management 46 (2005) 2996-3013.
[14] Maaß, C, U Schumann. 1996. Direct numerical simulation of separated turbulent flow over a wavy boundary. Notes on numerical fluid mechanics 52:227-241.
[15] T.S. Park, H.S. Choi, K. Suzuki, Nonlinea k-ε model and its application to the flow and heat transfer in a channel having one undulant wall, Int. J. Heat Mass. Transfer. 47 (2004) 2403-2415.
[16] K. Hafez, O. Elsamni, K. Zakaria, Numerical investigation of the fully developed turbulent flow over a moving wavy wall using k-ε turbulence model, Alexand. Eng. J. (2011).